TRANSPORT PHENOMENA AT INTERSECTIONS OF PRESSURIZED PIPE SYSTEMS

[1]P. Romero-Gomez, [1]C. Y. Choi, [2]B. van Bloemen Waanders, and [2]S. McKenna
[1]Department of Agricultural and Biosystems Engineering
The University of Arizona, Tucson, Arizona
[2]Sandia National Laboratories, Albuquerque, NM
Email addresses: P. Romero-Gomez, pedromer@email.arizona.edu, C. Y. Choi, cchoi@arizona.edu, B. van Bloemen Waanders, bartv@sandia.gov , and S. McKenna, samcken@sandia.gov.

Abstract

The movement of chemicals or biological agents in a water distribution system is examined via computational fluid dynamics simulations. A series of computational simulations using selected intersecting geometries are carried out at various Reynolds numbers. Boundary conditions, turbulence intensities, convergence criteria, and mesh sizes are thoroughly evaluated. The present parametric study focuses particularly on pipe intersections to characterize complex mixing phenomena in pressurized water distribution pipe networks. Selected computational results are compared with experimental results. The water quality model integrated with an existing computer program (EPANET) was re-evaluated based on the computational and experimental data. Initial computational fluid dynamics simulations consistently underestimated mixing, and experimental data are utilized to reexamine turbulent mixing by adjusting the turbulent Schmidt number. Corrections based on computational results are incorporated into the existing code as an example case study. The improvement of the existing code may be important not only to predict concentrations of chemical species such as chlorine in water distribution systems, but also to prepare for potential intentional and accidental contamination events. Computational results must be further calibrated and verified through lab- and field-scale experiments.

Keywords: transport phenomena, cross junction, water quality model, computational fluid dynamics.

1. Introduction

Accurate water quality descriptions in distribution systems are relevant to public health issues. The potential effects of drinking contaminated water are closely linked to the level of exposure to chemicals and biological contaminants. Researchers have used mass balance equations for the description of species spread (Rossman et al. 1993; Rossman et al. 1996; Uber et al. 2004). One major challenge includes the accurate modeling of species decay in the pipes due to bulk and wall reactions. Optimization techniques based on the intensive use of field data for calibrating models are used for solving this problem (Munavalli et al. 2003; Elton et al. 1995). Another recurrent concern is the computational resources spent on obtaining detailed, accurate results. Thus, computer modeling packages (e.g., EPANET, WaterCAD®, H_2ONet®, Pipe2000®, etc.) have been developed to simulate the potential hydraulic scenarios in a drinking water system. These packages are capable of performing both steady and extended-period (transient) simulations for the hydraulic and water quality analysis of pressurized pipe systems. Experience has proven that the hydraulic simulations are generally reliable.

Ratnayake and Jayatilake (1999) conducted a study on the performance of the existing water quality model to predict fluoride concentrations for a water distribution system under several scenarios. They concluded that the water quality might be used for the management of water quality in a water distribution system; however, their findings needed laboratory and field verifications. Uber et al. (2004)

stated that there are limitations to the existing computer water quality models due to the limited research and development carried out for the last 15 years. These limitations are more restrictive when modeling multi-component water quality levels and when several water sources interact in a system.

The accuracy of chemical transport in network models for small geometric configurations was examined by van Bloemen Waanders et al. (2005). Using experimental data (with NaCl) and two-dimensional computational fluid dynamics (CFD) simulation tools, they noted that the simplified assumption of complete mixing at pipe junctions in current water quality models might cause significant inaccuracies. They tested cross-joint mixing by introducing a tracer at the inlet boundary condition, while pristine water entered the other inlet. The exit concentrations are approximately 0.85 and 0.15, as opposed to 0.5, the expected value based on the perfect mixing assumption. Their findings are important for predicting dispersion patterns of chemical and biological species through multiple cross junctions in water distribution systems, as shown in Figure 1a. Cross junction joints (Figure 1b) are common, and they can be simplified to two- and three-dimensional shapes (Figures 1c and 1d) Further research is necessary to understand the water flow and mixing patterns of chemical and biological agents at various flow rates and geometries. In this study, therefore, we focus on mixing patterns at a cross intersection using Computational Fluid Dynamics (CFD) and experimental validation. Based on these results, the existing water quality model code is modified and compared with the results with the current water quality model. A widely-used open source code, EPANET, is used for the modification of the water quality code for the present study. It should be noted that we tested other commercial packages and obtained similar water quality outcomes due to perfect mixing assumptions.

The first part of this work consists of a thorough investigation of the most relevant parameters that allow us to perform a reliable numerical study; e.g., convergence criteria, mesh size, discretization schemes and boundary conditions. Next, results are presented for the turbulent Schmidt number, which is investigated by adjusting the numerical outcomes based on experimental data. Sodium chloride (NaCl) is used to simulate the dispersion patterns of target biological agents or chemical species, including chloramine and chlorine, in drinking water systems. Based on geographic notations, (*E, W, N,* and *S*) as presented in Figure 2, a dimensionless concentration is defined as:

$$C^* = \frac{C - C_W}{C_S - C_W} \tag{1}$$

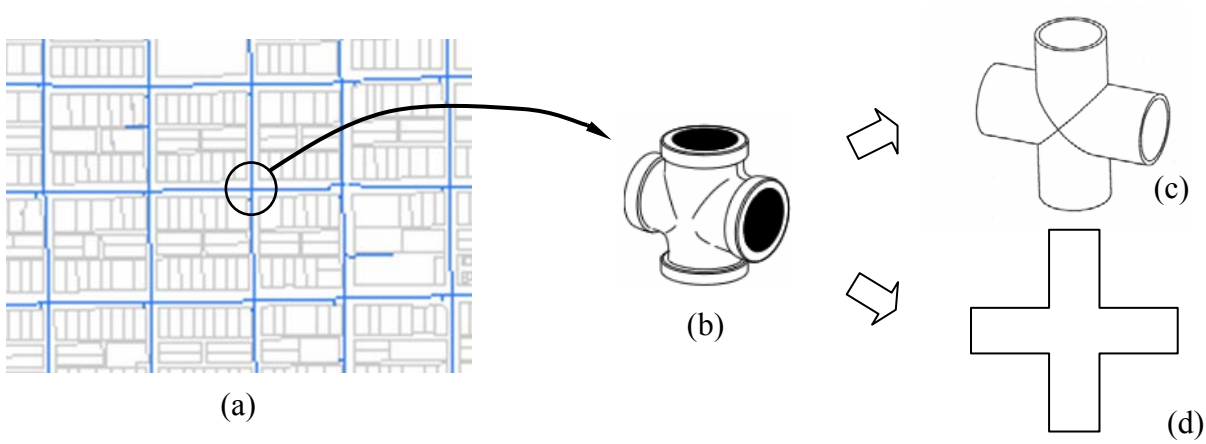

Figure 1. (a) A water distribution system featuring a cross junction in a mid-town neighborhood (Tucson, Arizona; courtesy of Tucson Water), (b) a typical cross-junction connector, (c) an idealized three-dimensional shape, and (d) a two-dimensional simplification.

The mixing can also be measured in terms of the split of incoming NaCl mass rate for any of the two outlets as:

$$\% \ NaCl_{E \ or \ N} = 100 \times \frac{\dot{m}_{E \ or \ N}}{\dot{m}_S + \dot{m}_W} \tag{2}$$

Perfect mixing at the junction would result in dimensionless concentrations equal to 0.5, or 50% NaCl at both outlets under certain conditions. The water quality model is generally based on this perfect-mixing assumption. However, the validity of this assumption is challenged and may be drastically altered depending on various parameters, notably geometry and flow speed. As a first step to address these parameters, three scenarios are suggested for a cross junction with the same pipe diameters as shown in Figure 2:

- **Scenario 1:** Equal inflows and outflows ($Re_S = Re_W = Re_N = Re_E$)
- **Scenario 2:** Equal outflows, varying inflows ($Re_S \neq Re_W$, $Re_N = Re_E$)
- **Scenario 3:** Equal inflows, varying outflows ($Re_S = Re_W$, $Re_N \neq Re_E$)

For the second scenario, the Reynolds numbers at both outlets were equal, and the Reynolds numbers at the inlets were different. The ratio of the inlet Reynolds numbers are defined as:

$$\mathrm{Re}_{S/W} = \frac{\mathrm{Re}_S}{\mathrm{Re}_W} \tag{3}$$

For the third scenario, the Reynolds numbers at both inlets are equal, whereas the Reynolds numbers at the outlets are different. Thus, the ratio of the exit Reynolds numbers are defined as:

$$\mathrm{Re}_{E/N} = \frac{\mathrm{Re}_E}{\mathrm{Re}_N} \tag{4}$$

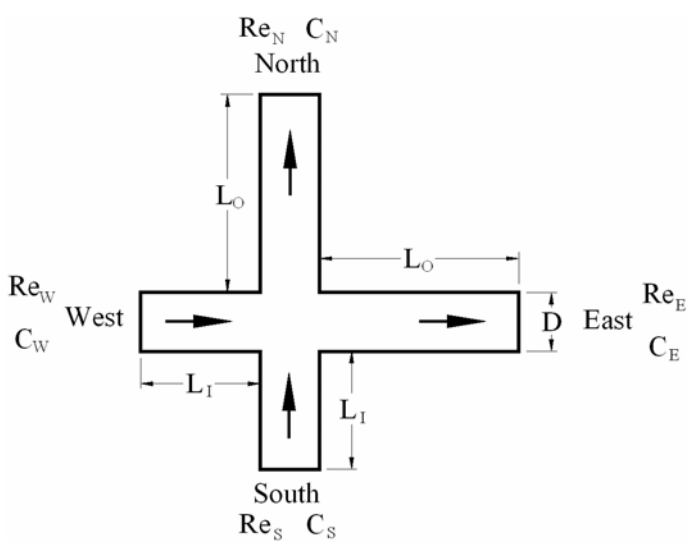

Figure 2. Hydraulic and water quality configurations of the flow at a cross junction.

2. Governing Equations and Boundary Conditions

The steady-state continuity and momentum equations were used to calculate the flow field. The incompressible conservation equations are as follows:

$$\nabla \cdot \bar{u} = 0 \tag{5}$$

$$\left(\nabla \cdot \bar{u}\bar{u}\right) = \frac{1}{\rho}\left[-\nabla P + \nabla \cdot (\bar{\bar{\tau}}) \right] \tag{6}$$

where $\bar{\bar{\tau}}$ is the stress tensor, which accounts for the effects of viscosity and volume dilation. No mass or momentum sources were considered and the field force and gravity were neglected. Turbulence was calculated by using the k-ε model, which is composed of two equations that account for the turbulence kinetic energy (k) and its rate of dissipation (ε):

$$\frac{\partial}{\partial x_i}\left(\rho k u_i\right) = \frac{\partial}{\partial x_j}\left[\left(\mu + \frac{\mu_t}{\sigma_k}\right)\frac{\partial k}{\partial x_j}\right] + G_k - \rho\varepsilon \tag{7a}$$

$$\frac{\partial}{\partial x_i}\left(\rho \varepsilon u_i\right) = \frac{\partial}{\partial x_j}\left[\left(\mu + \frac{\mu_t}{\sigma_\varepsilon}\right)\frac{\partial \varepsilon}{\partial x_j}\right] + C_{1\varepsilon}\frac{\varepsilon}{k}G_k - C_{2\varepsilon}\rho\frac{\varepsilon^2}{k} \tag{7b}$$

The eddy viscosity and turbulent production terms are modeled as follows:

$$\mu_t = \rho C_\mu \frac{k^2}{\varepsilon}, \quad G_k = -\rho\overline{u'_i u'_j}\frac{\partial u_j}{\partial x_i} \tag{8}$$

where the dimensionless constants for the turbulent model are: $C_{1\varepsilon} = 1.44$, $C_{2\varepsilon} = 1.92$, $C_\mu = 0.09$, $\sigma_k = 1.0$, and $\sigma_\varepsilon = 1.3$. In modeling turbulence, the effects of buoyancy, and incompressible turbulence, turbulence kinetic energy and dissipation rate source terms were neglected. The species transport was modeled by assuming NaCl is a passive scalar, i.e., it has no dynamic effect on the fluid flow (Warhaft, 2000). Thus, the solver calculated the velocity and turbulence fields, which were used to solve for the species distribution in the computational domain. Neglecting any chemical reaction and source terms, the steady-state species transport equation is as follows:

$$\rho \nabla \cdot \left(\bar{u}\, Y_i\right) = \nabla \cdot \left(\rho D_{AB} + \frac{\mu_t}{Sc_t}\right)\nabla Y_i \tag{9}$$

The right-hand side of Eq. (9) is the spatial gradient of the mass diffusion for turbulent flows, which is composed of the molecular and turbulent diffusions. The flow regime analyzed in this study is fully turbulent. Consequently, it is expected that eddy diffusivity dominates molecular diffusivity in the entire domain. Based on similarities to the laminar regime, eddy diffusivity is related to eddy viscosity through the turbulent Schmidt number:

$$Sc_t = \frac{\mu_t}{\rho D_t} \tag{10}$$

The boundary conditions are summarized in Table 1. The lengths of East and North pipes (L_O in Figure 2) were tested in order to avoid recirculating flow from the cross junction toward the outlet. Accordingly, the ratio L_O/D was set as 8. The ratio of the inlet's length to the diameter (L_I/D) was equal to 2.

3. Computational Approach

Convergence Criteria

In order to converge the iterative process within an acceptable error tolerance, the scaled residuals of the variables involved must be equal to or lower than the prescribed convergence criteria. The convergence criteria were set equal for all the conservation equations; they ranged from 10^{-2} to 10^{-7}. The scaled residuals for all the variables are calculated at each iteration.

The algebraic expression resulting from the discretization of the conservation equation for any modeled variable ϕ is as follows:

$$a_P \phi_P = \sum_{nb} a_{nb} \phi_{nb} + b \tag{11}$$

where a_P and ϕ_P are the coefficient and value of the variable ϕ at the cell center. a_{nb} and ϕ_{nb} come from the influencing neighbor cells and b is mostly influenced by the boundary conditions and source terms, if any. The scaled residuals (R^{ϕ}) to be compared to the convergence criteria result from the imbalance of Eq. (11), and are as follows:

$$R^{\phi} = \frac{\sum_{cells\ P} \left| \sum_{nb}\ a_{nb}\, \phi_{nb} + b - a_P \phi_P \right|}{\sum_{cells\ P} \left| a_P\ \phi_P \right|} \tag{12}$$

Mesh Generation

Among the characteristics of the computational mesh, the shape and number of elements are considered the most relevant parameters for accuracy. In this work, several mesh sizes were tested in order to define their influence on the numerical solution. The size ranged from 2,064 elements, which was about the same number used by van Bloemen Waanders et al. (2005) with MP Salsa based on Finite Element Method, up to 80,064 for 2D problems. Optimal mesh size is where any increase in the number of elements produces no noticeable change in the outcomes. Since the geometry of the pipes was very regular, quadrilateral elements were used over the entire computational domain.

Table 1. Boundary conditions for numerical simulation of the cross junction

	Velocity BC	Turbulence BC	Species BC
West inlet	$u = u_O,\ v = 0$	$I = I_o,\ L = D$	$Y = Y_O$
South inlet	$u = 0,\ v = v_O$	$I = I_o,\ L = D$	$Y = 0$
East outlet	$\frac{\partial u}{\partial x} = 0,\ \frac{\partial v}{\partial x} = 0$	$\frac{\partial k}{\partial x} = 0,\ \frac{\partial \varepsilon}{\partial x} = 0$	$\frac{\partial Y_i}{\partial x} = 0$
North outlet	$\frac{\partial u}{\partial y} = 0,\ \frac{\partial v}{\partial y} = 0$	$\frac{\partial k}{\partial y} = 0,\ \frac{\partial \varepsilon}{\partial y} = 0$	$\frac{\partial Y_i}{\partial y} = 0$
Walls	$u = 0,\ v = 0$	*Enhanced Wall Treatment*	$\frac{\partial Y_i}{\partial n} = 0$ *

* n = normal vector to the wall

Effects of Discretization Scheme

Numerical methods applied to the conservation equations are based on several discretization techniques. As a consequence, a particular technique has a set of corresponding solutions. There may be similarities in the solutions from some discretization schemes, whereas there may be significant differences from others. Four schemes were tested when the Reynolds number was equal to 44,000 at all inlets and outlets. The aim was to quantify the effect of each scheme on the mass rate split.

Two- and Three-Dimensional Approaches

In numerical modeling, a recurring question is whether a problem can be simulated in two-dimensions rather than three-dimensions with no significant effect on the outcomes. Dropping one independent spatial variable not only simplifies the conservation equations to be manipulated, but also dramatically reduces the computational time spent to obtain the solution (Romero-Gomez, 2005). Therefore, a three-dimensional mesh with 109,824 elements was created, and simulations were performed in order to compare the outcomes to those generated with a comparable two-dimensional mesh. The Reynolds number was the same for all inlets and outlets, ranging from 11,000 to 88,000. The 3D boundary conditions remained the same as for the two-dimensional scheme.

Effects of a Bump

Turbulence is induced by different means. The increased wall roughness contributes to increased turbulence intensity to some extent along with the changes in geometry due to fittings. Wall surfaces are assumed to be smooth**,** and thus the wall roughness is not considered throughout this study. Near the junction cross, on the other hand, fittings may create either gaps or bumps which may change turbulent intensity and the corresponding NaCl constituent mixing ratio. For this reason, different sizes of bumps were examined by creating a geometrical shape as depicted in Figure 3. The mass rate split was calculated with respect to the ratio of the reduced diameter (D_b) to the pipe diameter (D) at various L_b and W_b.

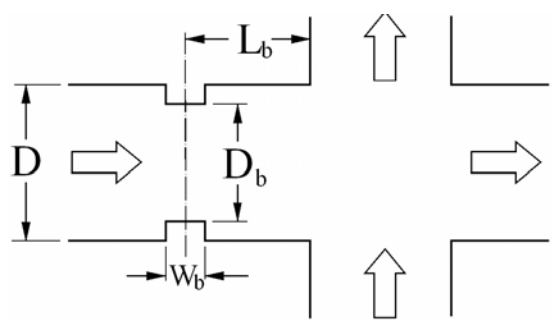

Figure 3. Geometry of a fitting at the cross junction shown at one of the inlets

Turbulent Schmidt Number (Sc_t)

In a k-ε turbulent model given in Eq. (7a) and (7b), total diffusivity is considered to be composed of the molecular and eddy diffusivities. Equation (9) indicates that the eddy diffusivity is calculated through the turbulent Schmidt number, whose definition is given in Eq. (10). Therefore, eddy diffusivity is directly proportional to the eddy viscosity computed at each node and inversely proportional to the Sc_t. Up to now, the previous simulations were performed by using the default value assigned to the turbulent Schmidt number (0.7). This was, however, inconsistent with the experimental results obtained. In this study, the preliminary results for testing Sc_t were obtained in order to match the numerical outcomes to the

experimental results (see Section 2.3). The tests were performed for the case when the Reynolds number is the same at both inlets and outlets, as well as in a wide range of the Reynolds ratio ($0.25 < Re_{S/W} < 1.00$) defined in Eq. (3).

CFD Benchmarking

A CFD package, FLUENT® (Lebanon, NH), is used to examine the different parameters involved in this problem and to define their correct values for an appropriate description of the flow field and dispersion patterns of species. FLUENT® uses the finite volume method to solve partial differential equations for the present problem. The primary concept is based on the fact that the values of the conserved variables are averaged across the volume (Patankar, 1980), and the method does not require a structured mesh. Many commercial packages based on this computational method have been widely used in various research and commercial applications. Nevertheless, we conducted a thorough study to examine the accuracy of solutions for several benchmark problems with analytical solutions and/or experimental data. Romero-Gomez (2005) chose benchmark problems relevant to the present study. These problems include (i) heat and fluid flow solutions for laminar flow though a circular pipe, (ii) laminar and turbulent boundary layers over a flat plate, and (iii) natural convection heated from the bottom. The first problem is directly relevant to the present problem. The second problem in particular carefully examined the effects of turbulent intensity. The third problem addresses the delicate heat and momentum balance induced by natural convection. This problem was originally examined by Kim and Choi (1996) using an in-house finite volume code. It was found that computational solutions were in excellent agreement with experimental and analytical solutions for the onset of natural convection in fluid and porous media. The results using FLUENT® were satisfactory for all problems tested.

Implementation

The required computational time is estimated based on the convergence criteria. Any decrease in the convergence criteria conveys a significant increase in the time needed to obtain the results. Consequently, a set of optimal convergence criteria is sought which provides accurate solutions with no effect on the computational results. The results indicate that the minimum value of R^{ϕ} (Equation 12) that may be used is 10^{-3} for all the conservation equations, as further decreases do not produce any significant changes in the results.

Similarly, testing several mesh sizes is required because it gives an estimate of the time needed to perform the subsequent simulations. It is also known that the discretization error is reduced by increasing the grid size; however, there is a point where truncation errors are amplified by increasing the mesh size. Therefore, it is required to find an optimal number of elements in the computational domain. It was observed that the optimal value is about 63,000 elements for 2-D calculations (Figure 4).

The 2D results for the mass rate split with different discretization methods are presented in Table 2. The 1st order scheme produces outcomes that indicate more mixing. On the other hand, the 2nd order and Quick scheme produce similar outcomes that indicate less mixing. A scheme that provides higher-order accuracy is preferable; therefore, the 2nd order scheme was used for all the subsequent simulations, as it takes less computational time to perform the simulations as compared to the Quick scheme.

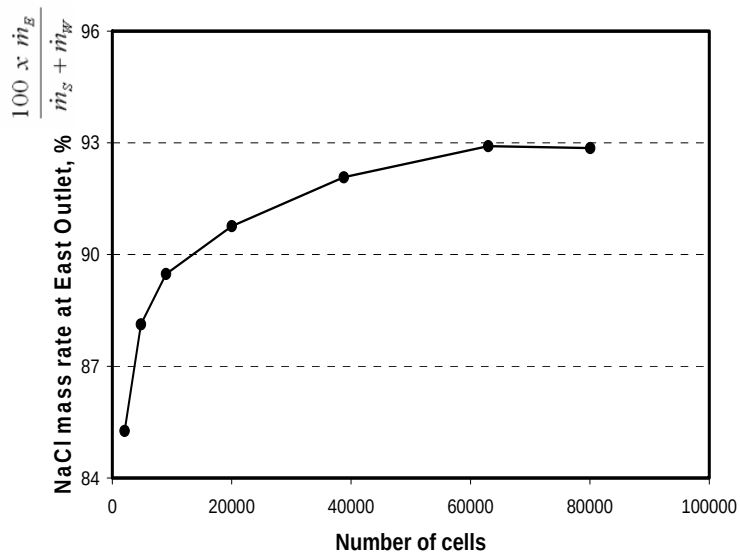

Figure 4. NaCl split with respect to the mesh size at the East outlet

Table 2. NaCl mass rate split under different discretization schemes (Scenario 1)

	NaCl mass rate %, East outlet	NaCl mass rate %, North outlet
1st order	92.9	7.1
2nd order	95.8	4.2
Quick scheme	95.7	4.3
Power law	94.2	5.8

The implementation of a bump due to fittings induces no significant increased mixing at the junction. It was observed that even when the diameter is reduced by 16% (D_b/D = 0.84, L_b/D=1, and W_b/D = 0.1) the mass split does not change significantly (approximately 2 % or less). In order to maintain a simple geometry, the pipes remained smooth (no bumps or gaps) for the subsequent simulations.

4. Experimental Setup and Preparation

To verify CFD results, a series of experiments were carried out at the University of Arizona, Tucson, Arizona. The experimental setup consisted of a cross-junction piping system with several sensors. The system included two pumps, two tanks, four gate valves and one cross junction with ¾ inch (1.905 cm) diameter pipes (Figure 5). Each of the two pumps delivered water from a separate tank; the water was then carried to the cross pipe intersection. A solution of NaCl was held in one of the tanks, while the other contained pure water. The concentration of NaCl was detected at three locations through sensors, along with the flow rate at four locations. Then, the amount of mixing at the cross junction was determined in relation to the Reynolds numbers, as defined in Eqns. (3) and (4).

The sensor data was taken in real time and averaged over a 20 s interval to represent one data point. This was intended to reduce the signal noise of the sensors and thus collect accurate and repeatable data. The

two primary sensor readings were flow rate and electrical conductivity. The flow rates were measured using paddle wheel sensors (FMK-515-3P3, the Omega Corporation, Stamford, Connecticut). Electrical conductivity, to determine the concentration of NaCl, was performed using four-ring potentiometric probes (CDE-1201, CDTX-1201, CDTX-1202, the Omega Corporation, Stamford, Connecticut). Currently, three types of flow scenarios have been investigated: equal inflows and outflows, equal outflows with varying inflows, and varying outflows with equal inflows.

The flow sensor error as described by the manufacturer is +/- 0.02 GPM (0.076 L/min) with a range of 1.7 to 34 GPM (6.44 to 128.7 L/min). The flow rates in the experiments were maintained above 1.7 GPM (6.44 L/min) and never approached 34 GPM (128.7 L/min) to ensure that the sensors functioned properly. Calibration of the flow sensors was done by timing and collecting the discharge as water was pumped at a constant rate through the sensors. A total of 25 points were collected for each flow sensor at varying flow rates.

The error of the electrical conductivity sensors as described by the manufacturer is +/- 2% of the full sensor range. Two different sensor ranges were used in order to minimize error: 0-200 mS/cm and 0-20 mS/cm. The 0-200 mS/cm range was used in the South and West pipes where sensor readings were expected to be greater. The 0-20 mS/cm range sensor was used in the North outlet where readings were expected to be lower. No electrical conductivity sensor was used in the East inlet as the concentration at this inlet was assumed to be zero since no salt had been added to the incoming water. Calibration was performed using commercially-prepared calibration solutions.

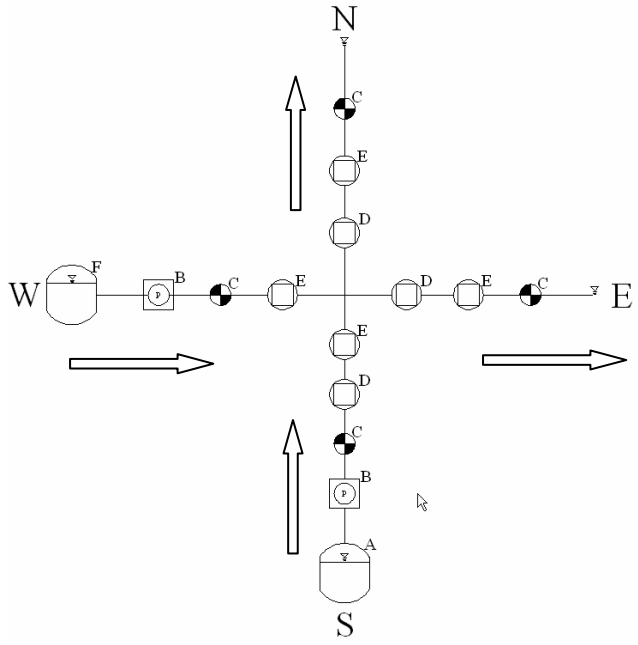

Figure 5. A schematic of the experimental setup. Key: (A) Saltwater Tank, (B) Pump, (C) Gate Valve, (D) Electrical Conductivity Sensor, (E) Flow Sensor, and (F) Freshwater Tank.

5. Experimental Results

Scenario 1: Equal inflows and outflows

For the case of fixed inflows and outflows, three separate trials have been conducted with a total of 40 data points. The average percent mass split calculated from the experimental data is 84.6 % and 16.5 % through the East and North outlets, respectively. There is a small amount of error due to the sensor readings, which accounts in part for the percentages adding up to slightly greater than 100 %. This percent mass rate split (i.e., 84.6 % and 16.5 %) is in excellent agreement with the one presented by van Bloemen Waanders et al. (2005); Scenario 1 is essentially a special case of Scenarios 2 and 3, and thus we included the experimental result by van Bloemen Waanders et al. (2005) in Figures 6 - 9.

Scenario 2: Equal outflows, varying inflows

For the case of equal outflows and varying inflows, the concentration ratio and the percent of mass rate split are quite different. As presented in Figure 6, the percentage of mass rate split reaches a maximum level around a Reynolds Number ratio of 0.7. It is logical that as $Re_{S/W} \rightarrow \infty$ the percent mass split will be 50%, because as $Re_{S/W} \rightarrow \infty$ only the saltwater inlet will have flow, and the salt will flow out of each outlet evenly. On the other hand, as $Re_{S/W} \rightarrow 0$ the percent mass split is expected to be 100%, because as the flow decreases in the saltwater inlet, it is logical that a higher percentage of the salt would be swept out the adjacent (East) outlet. This is not, however, what the experimental data suggests. It is quite possible that this trend is due to salinity sensor error. Sensor error becomes more pronounced at the extreme ends of the manufacturer's specified sensor range. When the extreme cases are tested, some of the sensors will be reading in a smaller range, so the percent error of these sensors is increased. Following the same logic as above, the overall trend for the dimensionless concentration does seem to be reasonable. This is because the sensor error is less pronounced by displaying the data in this fashion (Figure 7).

Scenario 3: Equal inflows, varying outflows

For the case of varying outflows with equal inflows, the trends are presented in very different ways when comparing the concentration ratio versus the percentage of mass rate split (Figures 8 and 9). Changing the outflow Reynolds numbers has a significant effect on the mass flow split. As the Reynolds number of an outlet is increased, the mass flowing through that outlet will also increase. In the case where $Re_{E/N} \rightarrow \infty$ the mass flow rate is expected to be 100%, because this would result in no flow through the North outlet and in all of the water and salt exiting through the East outlet. In the case of dimensionless concentration, the value should be 0.5, because the entire flow through the East outlet will result in half of the water coming from each inlet as the inlets Reynolds numbers are equal. As $Re_{E/N} \rightarrow 0$, the mass rate split through the East outlet is expected to be 0, because there will be no flow in the East outlet. It is expected that the dimensionless concentration will be close to 1 in this situation, because a very small flow through the East outlet would likely result in most of the flow through the East outlet coming from the adjacent (South) pipe.

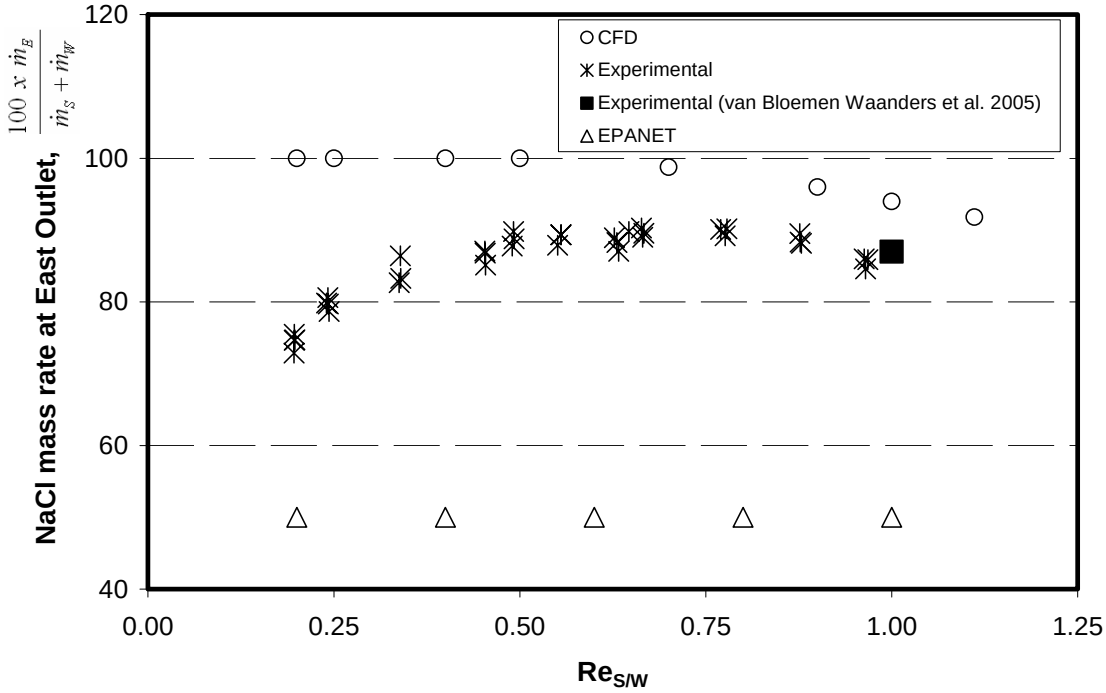

Figure 6. NaCl mass rate splits from the experimental, numerical and water quality model outcomes at different $Re_{S/W}$ (East Outlet), when $Re_S \neq Re_W$ and $Re_E = Re_N$.

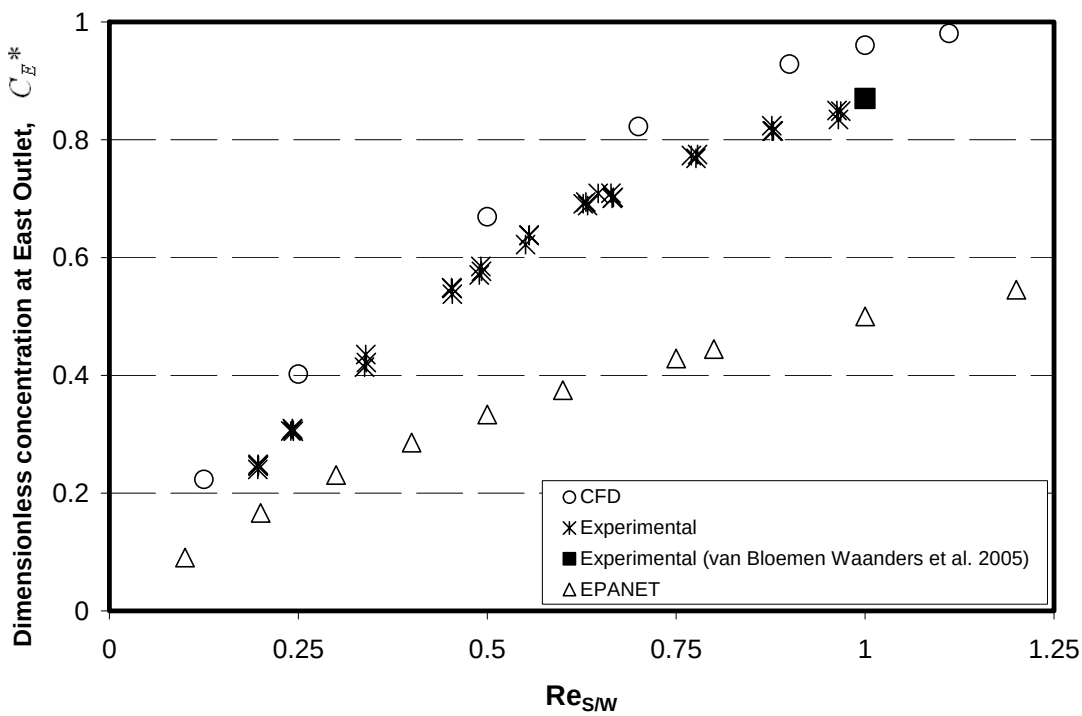

Figure 7. Dimensionless concentrations from the experimental, numerical and water quality model outcomes at different $Re_{S/W}$ (East Outlet), when $Re_S \neq Re_W$ and $Re_E = Re_N$.

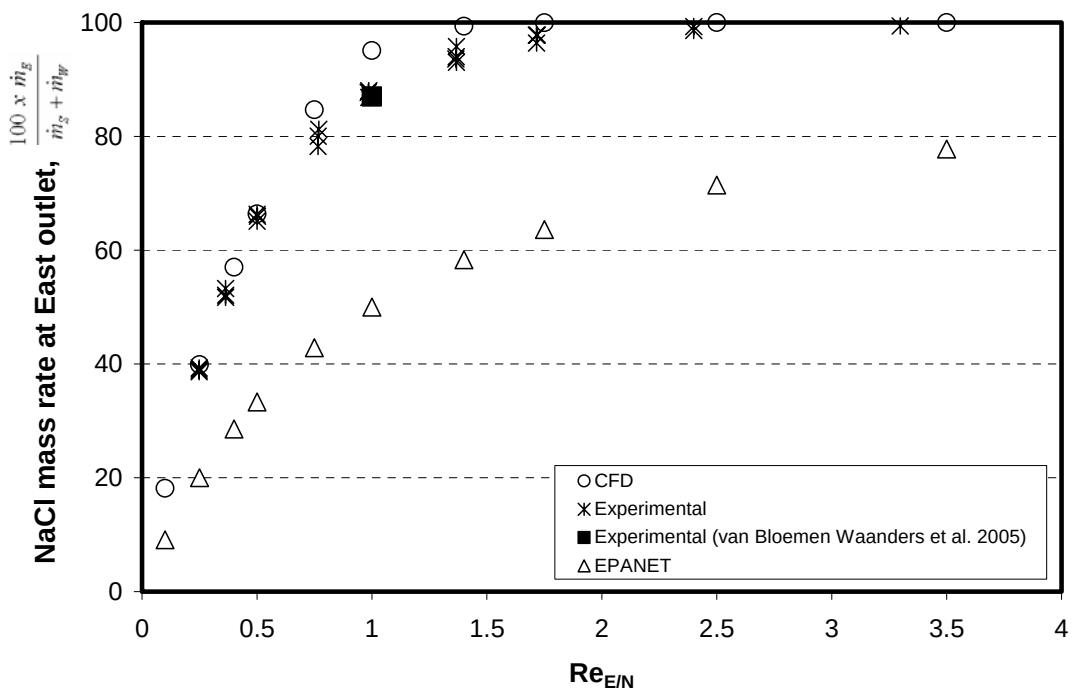

Figure 8. NaCl mass rate splits from the experimental, numerical and water quality model outcomes at different $Re_{E/N}$ (East Outlet), when $Re_S = Re_W$ and $Re_E \neq Re_N$.

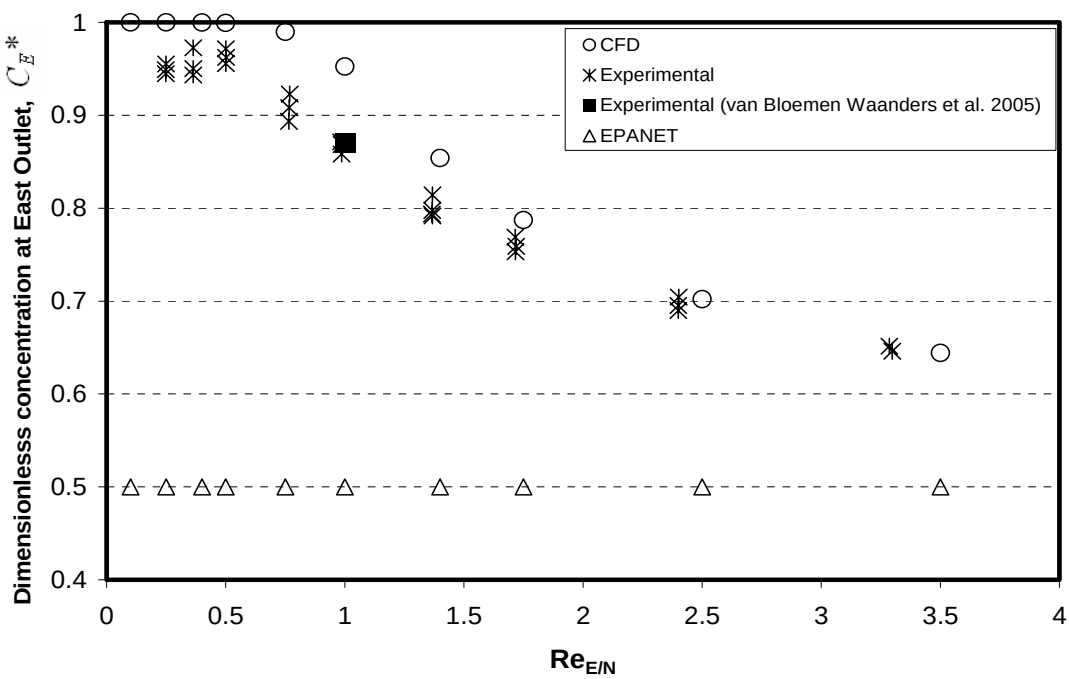

Figure 9. Dimensionless concentrations from the experimental, numerical and water quality model outcomes at different $Re_{E/N}$ (East Outlet), when $Re_S = Re_W$ and $Re_E \neq Re_N$.

6. Comparison of Computational and Experimental Results and Adjustment of Sc_t

In Figure 7, both the results for the experimental and numerical approaches are relatively close. However, the numerical outcomes are overestimated by about 10 % with respect to the experimental results throughout the entire range. On the other hand, the results obtained from the existing water quality model are underestimated by about 40% with respect to the experimental outcomes. The three data series converge as the value of Reynolds number ratio tends towards zero. This is due to little flow coming from the South inlet, which introduces the NaCl to the junction.

Figure 6 presents the same information as above, based on the split of NaCl mass rate, rather than dimensionless concentration. This plot shows different trends for each approach used. Numerical results present the most reasonable trends as $Re_{S/W} \rightarrow 0$ to 100 % NaCl mass rate, where the experimental measurement errors are significant, as discussed earlier; i.e., any NaCl entering at the South inlet flows out through the East outlet, with no mixing with the pure water flowing into the intersection through the West inlet. Water quality simulations using an existing EPANET model have a large error with respect to the experimental results. The NaCl mass split is constant and equal to 50% in the considered range, regardless of the Reynolds number ratio. The prediction of the same NaCl mass rate at both outlets is a clear indicator that the current water quality model assumes perfect mixing at the junction. This assumption, however, leads to an inaccurate description of the NaCl dispersion in a larger water network.

In Figure 9, the CFD outcomes are in good agreement with the experimental data series. Overall, numerical results overestimated C_E* in the given range of $Re_{E/N}$ (0.1 - 3.5), with a maximum error of about 9 % with respect to the experimental results. At higher $Re_{E/N}$, in particular, the experimental and computational data points nearly overlap. In contrast, the present water quality model produces the same concentration at the outlets regardless of the $Re_{E/N}$ due to the perfect mixing assumption. At higher values of $Re_{E/N}$, the incoming water flows out through the East outlet. Therefore, both experimental and computational data sets approach $C_E^* = 0.5$ as $Re_{E/N} \rightarrow \infty$.

In terms of the NaCl mass rate split, the CFD, experimental, and the results from the existing water quality model are shown in Figure 8. As expected, the NaCl mass rate split approaches 0% as $Re_{E/N} \rightarrow 0$, whereas it tends to 100% as $Re_{E/N} \rightarrow \infty$. The CFD results are slightly larger than the experimental mass rate split, being more pronounced in $0.75 < Re_{E/N} < 2$. Outside that range, the CFD results are in excellent agreement with the experimental ones. Calculations by the water quality model largely underestimated the mass rate split. In comparison with the experimental data, the CFD results for all cases consistently overestimated both mass split ratios and dimensionless concentration values. Overall, the discrepancy is due to less mixing modeled with the CFD default setting, which must be reexamined. On the other hand, the model produced significantly underestimated outcomes due to the perfect mixing assumption at the cross junction.

A major advantage of the CFD approach is that it enables us to analyze flow and mass transport phenomena in detail. For example, Figure 12a shows the contours of the NaCl concentration and vectors of the velocity magnitude, when the $Re_S = Re_W = Re_E = Re_N = 44{,}000$ (i.e., Scenario 1), and $D = 2$ in (5.08 cm). The NaCl concentration ranges from 0 to 0.01 kg NaCl /L throughout the domain, and the largest gradients occur along the line where the two incoming flows merge along the line AB in Figure 12a, where the mixing of the two sources of water occurs. The water at high concentrations (South inlet) interacts along a very narrow mixing strip with the incoming pure water (Left inlet), as if two impinging jets bounced off along AB as shown in Figure 12b. The velocity vectors in the computational domain are nearly symmetrical with respect to line AB because the hydraulic conditions at the inlets and outlets are the same for this particular case (Scenario 1). Based on experimental data, increased mixing is expected to occur when the eddy diffusivity increases at this narrow mixing zone. As expressed in Eq. (9), decreasing

the turbulent Schmidt number (Sc_t) or increasing eddy viscosity (μ_t) is one way to enhance turbulent eddies.

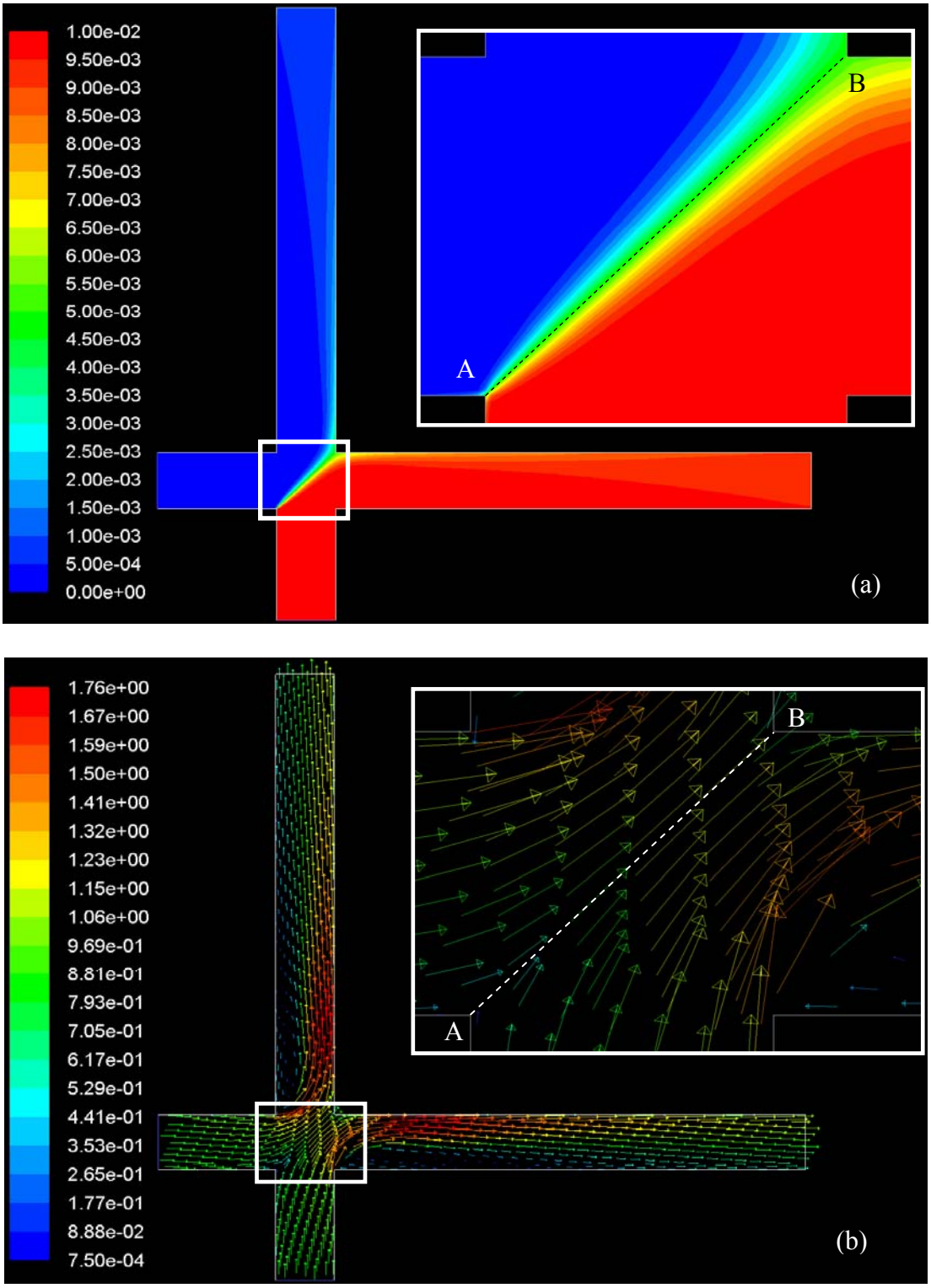

Figure 10. (a) NaCl concentration contours and (b) velocity vectors at the cross junction, when the *Re* is the same at all the inlets and outlets (*Re* = 44,000).

Thus, we postulated that the turbulent Schmidt number (Sc_t) has a major influence on the mixing phenomena at a cross junction. All the preceding simulations were performed with $Sc_t = 0.7$, which is the default value assigned by FLUENT® when a k-ε model is used. The difference between the outcomes from both approaches, however, may be fixed by adjusting Sc_t values. Therefore, as an example, various Sc_t values were tested until the NaCl split at $Re_{S/W} = 0.9645$ was equal to the experimental results under the same flow configuration. The resulting Sc_t was equal to 0.135, which is then used for simulations of $0.33 \leq Re_{S/W} \leq 0.96$. As shown in Figure 11, the modified CFD results are good agreement with the experimental data. Further investigation for adequate Sc_t is needed based on experimental data in comparison with CFD simulations. It should be noted that Ho *et al.* (2006) calibrated appropriate scaling of the tracer diffusivity based on results of experiments using cross-junction and double-T configurations. They presented that the turbulent Schmidt number needed to be reduced to a value of ~0.01 to account for enhanced mixing caused by instabilities and vortical structures along the interface of impinging flows.

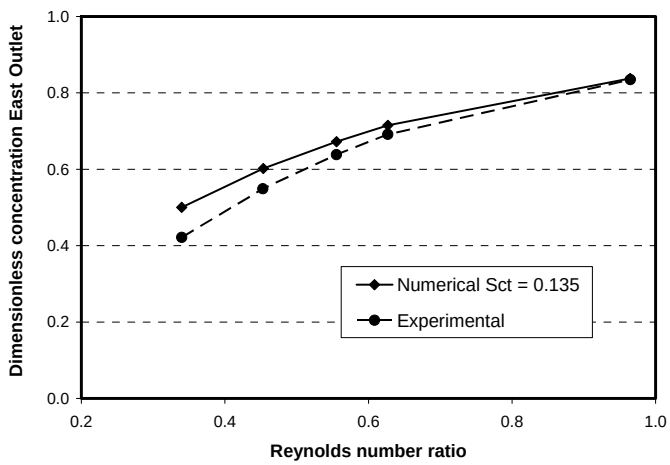

Figure 11. Dimensionless concentration of the experimental and numerical results with corrected Turbulent Schmidt Number (Sc_t) for the East Outlet when $Re_S \neq Re_W$ and $Re_E = Re_N$ (Scenario 2).

7. Modification of Water Quality Model - An Exemplary Case

A 5 x 4-node network was prepared as shown in Figure 12b based on a mid-town water distribution network in Tucson, Arizona (Figure 12a). There were a total of 5 instances in which the cross junctions had 2 inlets and 2 outlets (nodes 1- 5, excluding node 6 in Figure 12b). For each of these cases, the pipes had different Reynolds numbers. Simulating each cross junction separately in an experimental setup would be difficult because of the differing Reynolds numbers, so this network was simulated using CFD for each of the 5 specific junctions. Note that the adjustment of Sc_t was not made for this example.

In the current EPANET water quality model, mixing is assumed to be complete and instantaneous. According to Rossman (2000), for a specific node k, the concentration is as follows:

$$C_{i|x=0} = \frac{\sum_{j \varepsilon I_k} Q_j C_{j|x=L_j} + Q_{k,ext} C_{k,ext}}{\sum_{j \varepsilon I_k} Q_j + Q_{k,ext}} \tag{13}$$

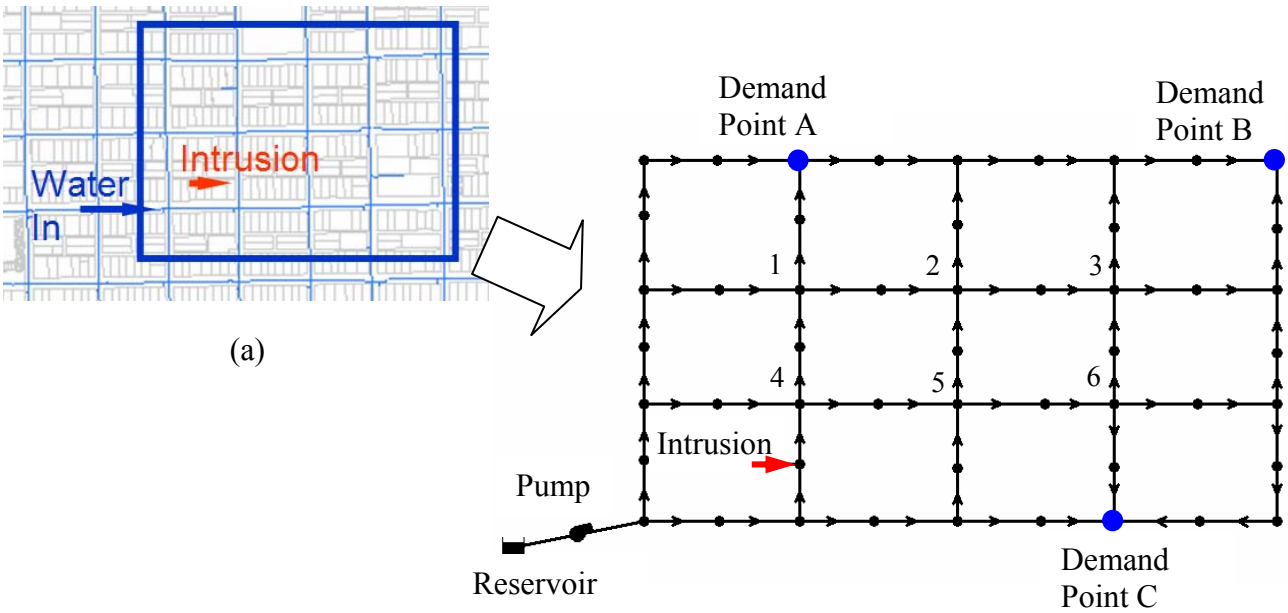

Figure 12. Scenario building and corresponding EPANET setup; (a) typical mid-town water distribution network and (b) a simplified water distribution network for an example case.

where i = link with flow leaving node k, I_k = set of links with flow into k, L_j = length of link j, Q_j = flow (volume/time) in link j, $Q_{k,ext}$ = external source flow entering the network at node k, and $C_{k,ext}$ = concentration of the external flow entering at node k. The notation $C_{i|x}=0$ represents the concentration at the start of link i, while $C_{i|x}=L$ is the concentration at the end of the link.

All of the nodes were assumed to be at the same elevation. The pump is a 1-point curve with a flow of 300 GPM (1135.6 L/min) and a head of 40ft (12.2 m). The pump provides pure water (C = 0 mg/L). The injection point injects a constant amount each hour: 100 mg/L of salt at 1 GPM (3.78 L/min). Subdivisions A, B, and C are demand points, each with a demand of 100 GPM (378.5 L/min). Each section of the pipe has a diameter of 12 in (30.48 cm), a roughness of 100 (HW), and a length of 500ft (152.4 m).

After the network was created and run in the steady-state mode in EPANET, the C/C++ code was modified so that each pipe displayed its corresponding Reynolds numbers. CFD simulations were carried out based on these Reynolds numbers. The dimensionless concentration splits were calculated and entered into the code. For each of the instances where a junction had 2 inlets and 2 outlets, CFD produced the corrected splits for each outlet, and the results were added to the existing water quality model in the original code on a node-by-node basis. The CFD results should be further corrected based on experimental results using the appropriate Sc_t, and the entire procedure is described in Figure 13.

When the modified code was used, the steady-state concentrations at Demand Points A, B, and C all displayed sizeable changes, as summarized in Table 3. For Demand Point A, for example, the salt concentration was drastically reduced by almost 9 times. For Demand Point B, the salt concentration was slightly elevated. For Demand Point C, the salt concentration was increased by nearly twice its original amount. Similarly, the mass rates changed significantly.

Figure 14 demonstrates concentration contours for the system. The concentration was evenly spread throughout the neighborhood using the original water quality model. Demand points A and C received a low amount, while the point B received a moderate concentration level. However, after the modified EPANET code was implemented using C/C++, the majority of the salt concentrations traveled to the Eastern part of the network. Demand point A barely received any salt, while demand points B and C had large increases in the amounts of salt. These results demonstrate that there are a lot of implications if the modified EPANET is used for solute transport for real world applications.

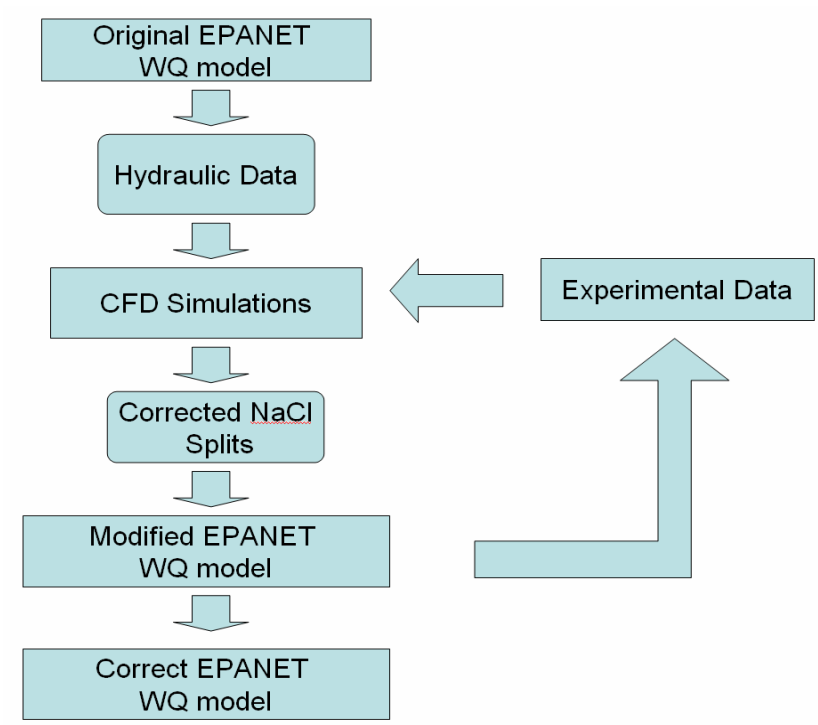

Figure 13. Flow chart of the procedure for improving the water quality model

Table 3. NaCl concentration (mg/L) and NaCl mass rate (mg/min) at Demand Points A, B, C using current and modified water quality model (total injected salt = 378 mg/min).

		A	B	C
NaCl concentration (mg/L)	Current	0.2699	0.5283	0.1489
	Modified	0.0303	0.6593	0.3598
NaCl mass rate (mg/min)	Current	102.02	199.70	56.28
	Modified	11.45	249.22	136.00

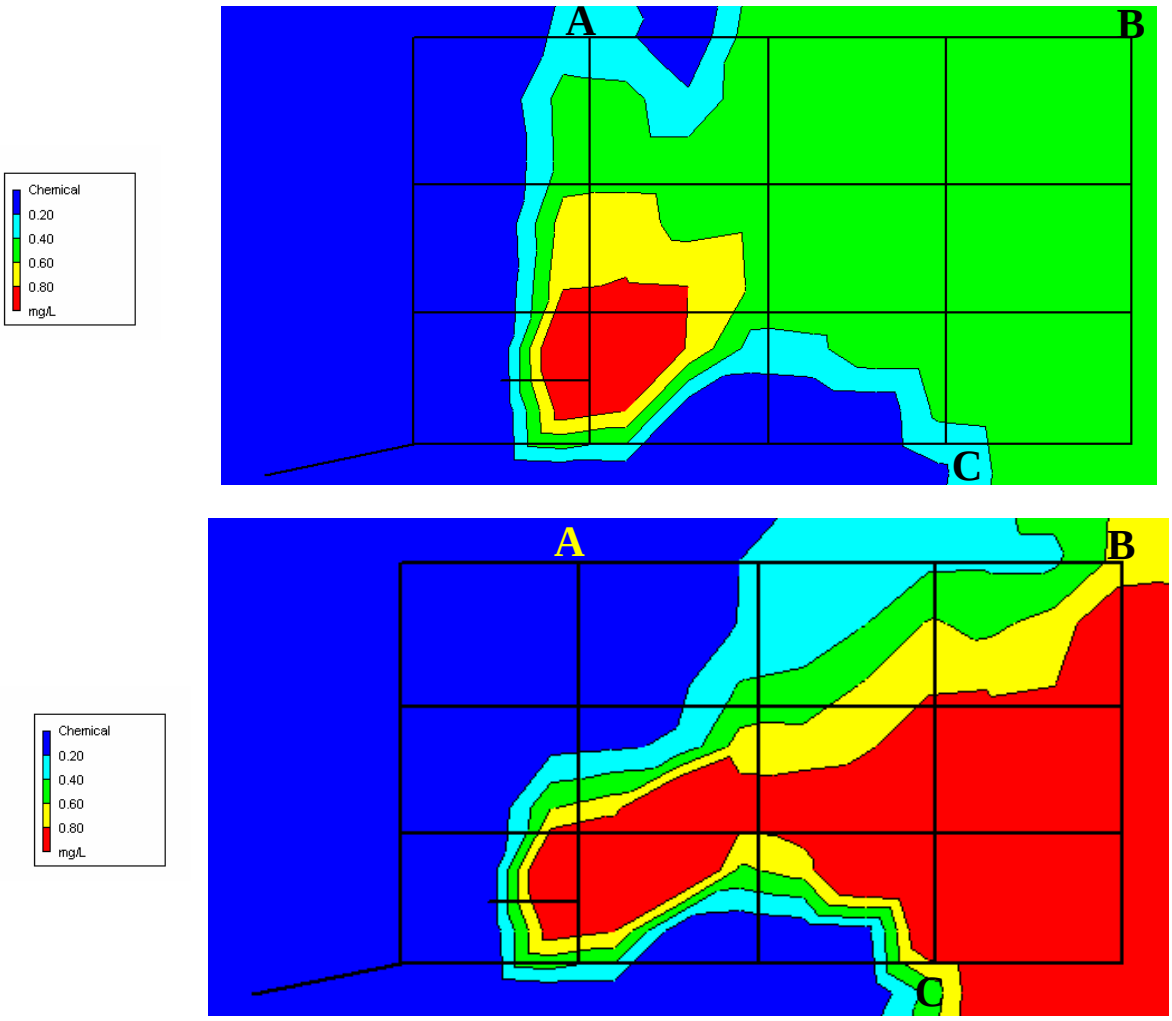

Figure 14. Contours of NaCl concentration (a) based on perfect mixing assumption and (b) after modifications of the code.

7. Conclusions and Recommendations

The present study addressed complex transport phenomena at four-pipe cross junctions, which are commonly found in municipal drinking water systems. Simulations using computational fluid dynamics (CFD), a series of experiments, and C/C++ programming were employed to address (i) existing problems based on the perfect mixing assumption in network water quality models and (ii) potential approaches for its revision. A series of additional computational and lab- and field-scale should verify the numerical results prior to the integration of the data into the water quality model. Eventually, the revised code should be generalized for various real-world cases.

The analysis presented in this paper is part of the efforts for an accurate modeling of water quality. As utilities change from having a single mission of supplying water to consumers to also having a security mission, the computer modeling tools used for network analysis will have to evolve to better simulate solute transport. The work presented here is an initial step in providing the experimental and CFD basis for improvements to these network analysis models. Solute mixing behavior at nodes will impact a wide variety of network analyses including prediction of disinfectant residuals, optimal locations for water

quality sensors, prediction models for early warning systems, numerical schemes for inverse source identification, and quantitative risk assessment.

Acknowledgements

This work is supported in part by the Environmental Protection Agency/Department of Homeland Security (under Grant No. 613383D) and in part by the National Science Foundation (under Grant No. EEC-0600855). We would like to acknowledge the many students and staff members at the University of Arizona (Susan and Neal O'Shaughnessy, Ryan Austin, Jerry Shen, and Levi Johnson), collaborators at Tucson Water (Dan Quintanar and Dean Trammel), and researchers at Sandia National Laboratories (Cliff Ho and Stephen Webb) who have contributed their valuable time and efforts to the present work.

References

Elton, A., Brammer, L.F., and Tansley, N.S. (1995). "Water quality modeling in distribution *networks." J. Amer. Water Works Assoc., 87(7), 44–52.*

Ho, C., O'Rear, L., Wright, J.L., McKenna, S.A. (2006). "Contaminant Mixing at Pipe Joints: Comparison between Experiments and Computational Fluid Dynamics Models." 8th Annual Water Distribution System Analysis Symposium, Cincinnati, Ohio, USA. Aug. 27-30.

Kim, S.J., and Choi, C.Y. (1996). "Convective heat transfer in porous and overlying fluid layers heated from below." *Int. J. Heat Mass Transfer* 39, 319-329.

Munavalli, G.R., and Kumar M. (2003). "Water quality parameter estimation in steady-state distribution system." *J. Water Resour. Plan. Management.,* 129(2), 124-134.

Patankar, V. (1980). *Numerical Heat and Mass Transfer.* Hemisphere, New York, N.Y.

Ratnayake, N. and Jayatilake, I. (1999). "Study of transport of contaminants in a pipe network using the model EPANET." *Wat. Sci. Tech*. 40(2), 115-120.

Romero-Gomez, P. (2005). *Modeling of natural ventilation rates for Mexican greenhouses.* MS thesis, Univ. of Arizona, Tucson, AZ.

Rossman, L., Boulos, P., and Altman, T. (1993). "The discrete volume-element method for network water quality models." *J. Water Resour. Plan. Management,* 119(5), 505–517.

Rossman, L., and Boulos P. (1996). "Numerical methods for modeling water quality in distribution systems: a comparison." *J. Water Resour. Plan. and Management.,* 122(2), 137–146.

Rossman, L. (2000). *EPANET-User's Manual*. United States Environmental Protection Agency (EPA), Cincinnati, OH.

van Bloemen Waanders, B., Hammond, G., Shadid, J., Collis, S., and Murray, R. (2005). "A Comparison of Navier-Stokes and network models to predict chemical transport in municipal water distribution systems." World Water and Envi. Resour. Congress, Anchorage, AL, May 15-19.

Uber, J., Shang, F., and Rossman, L. (2004). "*Extensions to EPANET for Fate and Transport of Multiple Interacting Chemical or Biological Components*." World Water and Envi. Resour. Congress, Salt Lake City, UT, June 27-July 1.

Warhaft, Z. (2000). "Passive scalars in turbulent flows." *Annu. Rev. Fluid Mech.* 32, 203-240.

Appendix. Notation

C = NaCl concentration, g/L
C^* = dimensionless concentration
D = pipe diameter, cm
D_b = reduced pipe diameter, cm
D_{AB} = molecular diffusivity, m/s^2
D_t = eddy diffusivity, m/s^2
I = turbulence intensity, %
k = turbulence kinetic energy, m^2/ m^2
L = hydraulic diameter, m
L_b = bump distance from intersection, cm
$\dot{m}$ = NaCl mass rate, g/s
P = pressure, Pa
R^ϕ = scaled residuals
Re = Reynolds number = $\rho u D/\mu$
Sc_t = turbulent Schmidt number
W_b = bump width, cm
$\bar{u}$ = velocity vector
u, v, w = velocity components, m/s
u', v', w' = fluctuating velocity, m/s
x_i = i-coordinate
Y_i = NaCl mass fraction to water mass, kg NaCl / kg water
ρ = density, kg/m^3
ε = turbulence dissipation rate, m^2/ m^3
μ = molecular viscosity, kg m^{-1} s^{-1}
μ_t = eddy viscosity, kg m^{-1} s^{-1}
%NaCl = percentage of outgoing NaCl with respect to total incoming NaCl, %

Suffix

0 = initial
E = east
I = inlet
N = north
O = outlet
S = south
W = west